Modelling of the viscoelastic behaviour with damage induced anisotropy of a plastic-bonded explosive based on the Microplane approach

Marwen Chatti, Arnaud Frachon, Michel Gratton, Michael Caliez, D. Picart, Nourredine Aït Hocine

Modelling of the viscoelastic behaviour with damage induced anisotropy of a plastic-bonded explosive based on the Microplane approach

M. Chatti[1*], A. Frachon[1], M. Gratton[1], M. Caliez[1], D. Picart[2], N. Aït Hocine[1]

[1]*INSA CVL, Univ. Tours, Univ. Orléans, LaMé, 3 rue de la Chocolaterie, BP 3410, 41034 Blois Cedex, France*

[2]*CEA DAM Le Ripault, F-37260 Monts, France*

[*]*Corresponding author: marwen.chatti@insa-cvl.fr*

Modelling of the viscoelastic behaviour with damage induced anisotropy of a plastic-bonded explosive based on the Microplane approach

M. Chatti[1*], A. Frachon[1], M. Gratton[1], M. Caliez[1], D. Picart[2], N. Aït Hocine[1]

[1]*INSA CVL, Univ. Tours, Univ. Orléans, LaMé, 3 rue de la Chocolaterie, BP 3410, 41034 Blois Cedex, France*

[2]*CEA DAM Le Ripault, F-37260 Monts, France*

[*]*Corresponding author: marwen.chatti@insa-cvl.fr*

Abstract. In this work, a mechanical constitutive law is proposed for a plastic-bonded explosive (PBX) which is a quasi-brittle energetic aggregate material, submitted to quasi-static loadings. Such material, sensitive to hydrostatic pressure, presents viscoelastic behaviour with damage induced anisotropy and irreversible strains. Previous models developed for this kind of material were mainly devoted for transient dynamic behaviour. The few existing quasi-static models considered the mechanical behaviour either isotropic or only elastoplastic. So, a new viscoelastic Microplane model with the damage induced anisotropy is proposed and implemented in commercial Finite Element software. The viscoelasticity was taken into account using a Maxwell generalized model with Microplane approach. The model consists in implementing the viscoelasticity inside the microplanes defining thus a Maxwell model on every direction. The sensitivity of the model to the strain increment magnitude and to the loading direction was analysed. As main conclusion, the experimental behaviour of the studied material was successfully predicted by this model.

Keywords: Plastic-bonded explosive, Microplane model, damage induced anisotropy, viscoelasticity

1 Introduction

Pyrotechnic structures constituted of plastic-bonded explosives (PBX) are commonly used in applications under quasi-static loadings, like storage and transportation. These applications induce high stress levels due to mechanical and/or thermal loadings that affect the material behaviour, which requires improved and accurate constitutive laws to simulate this

behaviour. Many models were developed in the last two decades for PBX materials, especially for dynamic and high-pressure loading conditions leading to ignition. The most popular is Visco-Scram (viscoelastic statistical crack mechanics) model (Bennett, et al., 1998). This model is a combination of the fragmentation theory proposed by Dienes from the early 80's (Dienes, 1982) (Dienes, 1996) (SCRAM) for brittle materials and viscoelastic Maxwell model (visco). The SCRAM approach consists of an isotropic model with the damage related to the mean crack radius, in which the growth rate is limited to a maximum value. An update was proposed afterward by Hackett & Bennett (Hackett & Bennett, 2000). They modified the crack growth law to consider the influence of the hydrostatic pressure on the damage and on the tensile and compressive responses. Recently, Xiao et al. (Xiao, et al., 2017) described the dynamic mechanical behaviour of PBX1314 as a function of aspect ratio and inclusion concentration. They modelled the viscoelastic behaviour of the polymer binder using a generalized Maxwell model, with a Prony series representation for the stress relaxation functions. Another damage constitutive model with viscoelastic response and statistical fracture was developed by Xiao et al. (Xiao, et al., 2017) to model low velocity impact experiment, for PBX. This model is based on SCRAM approach of Dienes (Dienes, et al., 2006) with a generalized Maxwell scheme. An isotropic constitutive relation is employed to describe the damage response of the material. For quasi-static loadings, Gratton et al. (Gratton, et al., 2009) developed an isotropic model assuming the material as damageable elastic viscoplastic. Then, an additional isotropic model that account for damageable viscoelasticity and plasticity was proposed by Le et al. (Le, et al., 2010) and Caliez et al. (Caliez, et al., 2014). The viscoelasticity was modelled using a generalized Maxwell chain model. Recently, Benelfellah et al. (Benelfellah, et al., 2014) and Picart et al. (Picart, et al., 2014) proposed an elastoplastic model with damage induced anisotropy, without considering the material viscosity. The authors illustrated the effect of the damage on engineering parameters and compared existing models based on the different aspects of the material behaviour. This investigation revealed that, among the constitutive laws proposed to model the anisotropic damage induced by the loading and satisfying the thermodynamic requirements, the Microplane approach, initially developed for concrete by Bazant & Gambarova (Bazant & Gambarova, 1984), provides a powerful framework to implement complex laws. Particularly, the introduction of a unilateral effect is possible keeping a non-dissipative free energy, a continuous stress–strain response or a symmetrical stiffness tensor (Benelfellah, et al., 2014). The Microplane-based models were successfully used to predict

viscoelastic behaviour of uncracked concrete, creep, rate dependence of crack growth, aging creep and creep-cracking interaction (Di Luzio & Cedolin, 2007) (Di Luzio, 2009) (Ozbolt & Reinhardt, 2001) (Ozbolt & Bazant, 1992) (Hasegawa & Bazant, 1993) (Bazant, et al., 2000). These models were developed following two approaches: "internal approach", where the viscoelasticity is integrated inside the microplanes (Zi & Bazant, 2002), and "external approach", where the viscoelasticity is defined in series with a damaged elastic Microplane model (Di Luzio & Cedolin, 2007) (Di Luzio, 2009). In the present paper, a constitutive law for a quasi-brittle energetic material submitted to quasi-static loadings, is proposed. This constitutive law accounts simultaneously for the viscoelasticity and the anisotropic nature of the damage, based on the Microplane approach.

Numerical aspects of microplane models didn't have the same interest as constitutive laws. Previous studies show an influence of strain increment magnitude and loading direction on the simulation results. In addition, the integration formula (number and weight of the microplanes for the spatial partition) has an important impact on the predictions of the models and depending on the number and the distribution of the integration points used, the influence can be very distinct (Badel & Leblond, 2004) (Ehret, et al., 2010) (Huang, et al., 2017) (Levasseur, et al., 2013) (Nemecek, et al., 2002) (Verron, 2015) (Qiu & Crouch, 1997). Thus, the sensitivity of the proposed model to the strain increment magnitude and to the loading direction is analysed using different integration formulas.

Numerical simulations achieved in this work are based on experimental data performed on a Plastic Bonded Explosive (PBX) and published in (Le, et al., 2010). This data includes monotonic and cyclic compression and tension, carried out at a strain rate of 3.3×10^{-5}/s, and monotonic compression, performed at strain rates of 8.3×10^{-4}/s and 4.4×10^{-6}/s. Experimental results showed a quasi-brittle nonlinear behaviour and a high dependency on the strain rate, hydrostatic pressure and temperature, which makes difficult the experimental investigation and modelling of the PBX behaviour.

2 Experimental investigation

The studied PBX material is made of more than 95% of energetic crystals (octahydro-1,3,5,7-tetranitro-1,3,5,7-tetrazocine, HMX) mixed with a low percentage of a polymer binder. The mixture is pressed using an isostatic compaction process that aims to eliminate the initial porosity of the powder. The final product was machined into solid samples of various shapes (Picart, et al., 2014). Optical microscopy observations showed the high solid fraction of

crystals whose size varies from a few tens of microns to a few hundred of microns, with an average size of 200 μm. The crystals have different forms and are randomly orientated in the material (Picart, et al., 2014). On the pristine material, optical microscopy observations highlighted the presence of a lot of pre-existing intra-granular microcracks and a lot of grain–grain surface contacts. However, after submitting the material to a low confinement, optical micrographs revealed loading induced intergranular and intra-granular microcracks, and straight bands related to inelastic deformation of some grains (Picart, et al., 2014) (Le, et al., 2010). PBX material presents a nonlinear behaviour, whatever the loading conditions, with asymmetry between tension and compression. A quasi-brittle behaviour is obtained during tensile tests while a more ductile one is observed during compression and triaxial tests. Due to the presence of polymer binder, the material presents strain rate and temperature dependencies (Le, et al., 2010) (Caliez, et al., 2014). Also, a dependency of the material behaviour, particularly the initial elastic modulus, on the confinement pressure is observed. This could be related to the closure of a part of initial porosity and the evolution of contact conditions between crystals with increasing hydrostatic pressure, as suggested by Caliez et al. (Caliez, et al., 2014) and Picart et al. (Picart, et al., 2014). Residual strains are registered after unloading and recovery and a hysteretic response are highlighted for cyclic loading. The observed broad loops and the decrease of the stress (respectively the strain) during the relaxation (respectively the recovery) conditions are attributed to viscoelastic behaviour of the material and probably internal friction (Picart, et al., 2014). The observations above prove that the studied material behaves like a concrete, due to its quasi-compact aggregate microstructure. The main difference with concrete is the strong temperature and strain-rate dependencies. The literature contains some studies on the strain rate dependent behaviour of PBXs (Ellis, et al., 2005) (Chen, et al., 2007) (Liu, et al., 2009) (Williamson, et al., 2008) (Le, et al., 2010). Viscoelastic behaviour of the material was characterized using DMA experiments allowing the determination of the storage and loss moduli (Le, et al., 2010). Analysing the results of cyclic compression and cyclic confined compression at hydrostatic pressure levels of 5 MPa and 10 MPa, Le (Le, et al., 2010) suggested that the studied PBX displays linear viscoelastic behaviour. Using these tests, and comparing the viscous stress at two levels of isovalues of global stress, Le (Le, et al., 2010) concluded that the viscoelastic part does not depend on the pressure. In some recent models, the behaviour of PBX materials was considered as anisotropic. Using a dynamic compression test on a Hopkinson bar Trumel et al. (Trumel, et al., 2010) showed the presence of a network of cracks that induces an

anisotropic degradation of the mechanical properties of the material. Unfortunately, the anisotropic nature of the damage could not yet be directly observed. Evidence of anisotropic damage is highlighted by the degradation observed on the longitudinal modulus and the called "transversal elastic modulus". Picart et al. (Picart, et al., 2014) reported the results of tension and compression experiments where the "transversal stiffness" of the studied PBX evolves faster in compression than in tension, which is in accordance with the idea of an anisotropic damage that preferentially occurs in mode I. This has been proved also using the evolution of the contraction ratio defined as the ratio of the transversal elastic strain and the longitudinal elastic strain $-\varepsilon_T^e/\varepsilon_L^e$. It appeared that this ratio varies from 0.28 to 0.75 for the studied PBX (Le, et al., 2010), while it should not exceed 0.5 in the isotropic framework. An explanation presented by Pecqueur (Pecqueur, 1995) after studying sandstone and then adopted by Dragon et al. (Bargellini, 2006) invokes damage induced anisotropy. If such anisotropic damage is macroscopically observed, its causes remain difficult to be identified. Nevertheless, this phenomenon was explained as the consequence of oriented microcracking process (Picart, et al., 2014). Previous works by Benelfellah et al. (Benelfellah, et al., 2014) and by Picart et al. (Picart, et al., 2014) also highlighted the damage effectivity of the PBX. In fact, tensile loading and compressive loading applied in the direction perpendicular to a "micro-crack" surface lead, respectively, to opening and closing of such a crack, which allows the recovery of the stiffness in the compression case.

3 Constitutive laws

In what follows, the Microplane approach and the damage evolution laws are presented. Then, the procedures and schemes used to model the viscoelasticity with the anisotropic damage are detailed. Finally, the identification procedure of the model material parameters is described.

3.1 Microplane approach and damage evolution law

As mentioned above, the material presents an evolving damage with induced anisotropy. Some procedures have been developed in the literature to model such damage (Maire & Chaboche, 1997) (Zhu, et al., 2008) (Bargellini, et al., 2008) (Murakami & Kamiya, 1997). However, despite continuous improvements of these procedures, inconsistencies remained in the used methods (Challamel, et al., 2006) (Cormery & Welemane, 2002) (Carol & Willam, 1996). The background of the Microplane approach can be traced back to Taylor (Taylor,

1938). The basic idea is that the stress-strain relations can be defined independently on various planes in the material. It was applied first to model the plasticity (Batdorf & Budiansky, 1949). The Microplane approach was proposed by Bazant et al. (Bazant & Gambarova, 1984) to simulate concrete material behaviour. This approach states that each direction of the solid angle characterizes a microplane on which the strain is decomposed (Figure 1). It should be noted that Microplane approach is not a micro-macro homogenisation model but rather a spatial partition. Constitutive equations are defined in the microplane level where the existence of free energy is assumed. The global stress tensor is determined by angular integration of the microplane stress vector over the whole solid angle. The global free energy ψ^{glo} is equal to the angular integral over the entire solid angle Ω of the angular free energy density, expressed as $\psi^i/4\pi$ and associated to each plane defined by its normal vector $\underline{n}^i$:

$$\psi^{glo} = \frac{3}{4\pi}\int_{\Omega} \psi^i(\underline{t}_\varepsilon, q)d\Omega, \qquad \text{(Eq. 1)}$$

where the subscript i denotes the microplane orientation, $\underline{t}_\varepsilon = \underline{\underline{\varepsilon}}.\underline{n}^i$ represents a deformation vector and q is a set of state variables.

The global stress tensor $\underline{\underline{\sigma}}$ is defined by the partial derivative of the free energy ψ^{glo} with respect to the strain tensor $\underline{\underline{\varepsilon}}$:

$$\underline{\underline{\sigma}} = \frac{\partial \rho_0 \psi^{glo}}{\partial \underline{\underline{\varepsilon}}} = \frac{3}{4\pi}\int_{\Omega} \frac{\partial \rho_0 \psi^i(\underline{t}_\varepsilon, q)}{\partial \underline{\underline{\varepsilon}}} d\Omega$$

It should be noted that variables underlined with one line are vectors, those underlined with two lines are twice rank tensors and those underlined with four lines are fourth rank tensors. Many different Microplane formulations exist in the literature, based on the strain decomposition (Normal-shear, volumetric-deviatoric, etc). Carol et al. (Carol, et al., 2001) proposed a thermodynamically consistent Microplane model with a Volumetric-Deviatoric-Tangential (V-D-T) split i.e. with a decomposition of the strain tensor to volumetric, deviatoric and tangential components respectively noted ε_V, ε_D and $\underline{\varepsilon}_T$ and expressed as follows in each microplane:

$$\varepsilon_V = \frac{1}{3}\underline{\underline{1}} : \underline{\underline{\varepsilon}} = \underline{\underline{V}} : \underline{\underline{\varepsilon}} \quad \text{(Eq. 2)}$$

$$\varepsilon_D = \left(\underline{n} \otimes \underline{n} - \frac{1}{3}\underline{\underline{1}} \right) : \underline{\underline{\varepsilon}} = \underline{\underline{D}} : \underline{\underline{\varepsilon}} \quad \text{(Eq. 3)}$$

$$\underline{\varepsilon}_T = \left(\underline{n} \cdot \underline{\underline{I}} - \underline{n} \otimes \underline{n} \otimes \underline{n} \right) : \underline{\underline{\varepsilon}} = \underline{\underline{T}} : \underline{\underline{\varepsilon}} \quad \text{(Eq. 4)}$$

Equations (2), (3) and (4) define the projection of the global strain tensor on a microplane. It should be noted that ε_V is isotropic in the material. These strains allow the determination of stresses in a microplane with the following state laws:

$$\sigma_V = \frac{\partial \rho_0 \psi^i (\underline{t}_\varepsilon, q)}{\partial \varepsilon_V} \quad \text{(Eq. 5)}$$

$$\sigma_D = \frac{\partial \rho_0 \psi^i (\underline{t}_\varepsilon, q)}{\partial \varepsilon_D} \quad \text{(Eq. 6)}$$

$$\underline{\sigma}_T = \frac{\partial \rho_0 \psi^i (\underline{t}_\varepsilon, q)}{\partial \underline{\varepsilon}_T} \quad \text{(Eq. 7)}$$

The global stress tensor is then evaluated from the stresses defined in microplanes by an integral over the solid angle Ω, using the following equation:

$$\underline{\underline{\sigma}} = \frac{3}{4\pi} \int_\Omega \left\{ \sigma_V . \underline{\underline{V}} + \sigma_D . \underline{\underline{D}} + \underline{\sigma}_T . \underline{\underline{T}} \right\} \quad \text{(Eq. 8)}$$

We should note that the operators used to get the global stress are the same used during the decomposition of the strain into the microplanes.

When the Microplane approach is used to model only damageable elasticity, a global potential can be expressed by integration by taking into account a damaged elastic global anisotropic operator. Microplane approach can be used in this case only to define this operator without introducing all the variables at the level of microplanes. To model the induced anisotropic damage of the material, the free energy is defined as follows (Picart, et al., 2014):

$$\psi^i = \frac{1}{2} E_V \left(1 - \alpha_V \left(\varepsilon_V\right) d_V\right) \varepsilon_V^2 + \frac{1}{2} E_D \left(1 - \alpha_D \left(\varepsilon_D\right) d_D\right) \varepsilon_D^2 + \frac{1}{2} E_T \left(1 - d_T\right) \underline{\varepsilon}_T . \underline{\varepsilon}_T \quad \text{(Eq. 9)}$$

In this equation, three damage variables d_V, d_D and d_T, that affect the corresponding elastic moduli denoted, respectively, E_V, E_D and E_T, are introduced. These moduli are related to the bulk and shear global parameters K and μ as follows: $E_V = 3K$ and $2E_D+3E_T = 10\mu$ (Carol, et al., 2001). The damage is calculated at the level of microplanes. d_V is the same for all

microplanes since ε_V is isotropic. d_D and d_T are calculated individually for each microplane, based on ε_D and $\underline{\varepsilon}_T$ (Eqs. (2), (3) and (4)). α_V *and* α_D are the effectivity functions defined, respectively, in terms of volumetric strain and deviatoric strain for each microplane. These effectivity functions manage the opening/closure of microcracks, asymmetry of the behaviour between tension and compression and the effect of hydrostatic pressure. It has been assumed that d_T is not affected by the effectivity. To avoid a spurious dissipation and discontinuity in the model responses and to obtain simple constitutive laws, α_V and α_D depend on their associated strain components. In the proposed model the damage depends on the total strain. The assumed relationships between damage variables and their associated forces F_V, F_D and F_T are given in terms of ε_V, ε_D and $\underline{\varepsilon}_T$ respectively for each microplane:

$$F_V = -\frac{\partial \rho_0 \psi^i}{\partial d_V} = \frac{1}{2} E_V \alpha_V \left(\varepsilon_V\right) \varepsilon_V^2$$

(Eq. 10)

$$F_D = -\frac{\partial \rho_0 \psi^i}{\partial d_D} = \frac{1}{2} E_D \alpha_D \left(\varepsilon_D\right) \varepsilon_D^2 \qquad \text{(Eq. 11)}$$

$$F_T = -\frac{\partial \rho_0 \psi^i}{\partial d_T} = \frac{1}{2} E_T \underline{\varepsilon}_T . \underline{\varepsilon}_T \qquad \text{(Eq. 12)}$$

Taking into account the effect of the pressure on the damage evolution and the dependency of this damage on strain, the following phenomenological relations have been proposed by (Picart, et al., 2014) in a microplane:

$$d_{V,D,T}\left(F_{V,D,T}, p\right) = \max\left(d^0_{V,D,T}, 1 - \exp\left[-p\left(a_1 F_{V,D,T}\right)^{a_2}\right]\right)_t, \; 0 \le d_{V,D,T} \le 1 \qquad \text{(Eq. 13)}$$

where:

$$p = 1 + \left[a_3 . H(-\varepsilon_V) + a_4 . H(\varepsilon_V)\right] E_V \left\langle \varepsilon_V - \varepsilon_V^{0-H10} \right\rangle_+ \qquad \text{(Eq. 14)}$$

The effectivity functions are defined as follows:

$$\begin{cases} \varepsilon_V \ge \varepsilon_V^{0-H10} \rightarrow \alpha_V\left(\varepsilon_V\right) = a_3 \\ \varepsilon_V \succ \varepsilon_V^{0-H10} \rightarrow \alpha_V\left(\varepsilon_V\right) = a_4 \end{cases}$$

$$\begin{cases} \varepsilon_D \ge 0 \rightarrow \alpha_D\left(\varepsilon_D\right) = 0.5 \\ \varepsilon_D \succ 0 \rightarrow \alpha_D\left(\varepsilon_D\right) = 1 \end{cases}$$

In the previous equations, a_j are four material parameters. a_1 and a_2 manage the evolution of the damage versus the strain, and a_3 and a_4 manage the dependency of the damage on the pressure. The pressure dependency is carried out through the function p given by equation

(14), where ε_V^{0-H10} is a third of the negative volumetric strain reached after hydrostatic compaction of 10 MPa. In this model (Picart, et al., 2014), the four material parameters a_j are the same for d_V, d_D and d_T. Nevertheless, the evolution law offers the possibility to use different values of a_1 and a_2 for d_V, d_D and d_T. The main limit of the models based on an additivity of oriented damages comes from the impossibility to experimentally identify the effect of each oriented microcracks group on the global mechanical response of the material. Thus, the parameters related to the damage evolution should be calibrated by comparing the numerical predictions of the material global behaviour to the test data.

3.2 Viscoelastic Microplane model

Many viscoelastic models exist in the literature. One of the commonly used models is based on the nonlinear viscoelastic model of Schapery identified for solid propellants which that have many similarities to PBX materials (Ha & Schapery, 1998). Belmas et al. (Belmas, et al., 1982) have modelled both linear and non-linear viscoelasticity of an explosive material composed of 90%wt of crystals. Linear viscoelasticity is generally defined in the low strain range while nonlinear viscoelasticity is defined in the large one. Based on the studies of Le (Le, et al., 2010) (Caliez, et al., 2014) and Belmas (Belmas, et al., 1982), the linear viscoelasticity would be convenient for the material studied in the present work. The generalized Maxwell model corresponds to a Prony series development for the relaxed moduli. It is considered as a sum of contributions or elements, each one consisting of a spring and a dashpot in series. In this context, the Maxwell chain is more effective than the Kelvin chain (Zi & Bazant, 2002). As mentioned above, two approaches exist to take into account such a kind of viscoelasticity with a Microplane model: external and internal approaches.

The external approach consists on defining in series the Maxwell model with a damaged elastic Microplane model. The damage is calculated with the Microplane model, whereas the elastic strains and stresses are obtained for viscoelastic elements and elastic element from the Maxwell chain model defined with the Microplane model. The Microplane model is used to generate the 11 damaged elastic operators. No other state variables but damage variables are introduced in the microplanes. The Microplane model yields a fourth rank damaged stiffness tensor $\underline{\underline{\underline{\underline{C}}}}^d$ calculated using elastic and viscoelastic moduli that affect all the mechanisms in the Maxwell model. Each mechanism contributing to the global behaviour is defined by an elastic strain tensor and its corresponding stress tensor. In this approach, elastic strains in the

elements of the Maxwell model are not projected on the microplanes and, so, they do not depend on Microplane directions.

The internal approach states that a viscoelastic law is integrated inside the microplanes, i.e each microplane contains a Maxwell chain model. The viscoelastic model is integrated in each microplane, following V-D-T decomposition, i.e a Maxwell chain model is defined along every direction, containing 10 viscoelastic elements and one elastic element. Defining the behaviour inside the microplanes requires the determination of the elastic strain and the elastic stress for every microplane direction and every element. By analogy with asphalt materials (Saadeh, 2005), the anisotropy of stiffness matrix due to damage is supposed to imply the anisotropy of relaxation times, while viscous moduli are considered to be constant through the time and through the solid angle. Only one set of damage variables (d_V, d_D and d_T) is introduced for the whole multi branch model (for the elastic and the viscoelastic parts). The damage evolution laws of d_V, d_D and d_T, in the viscoelastic model are non-associated: the damage depends only on the contribution of the associated force within the purely elastic element (total strain projected on the microplanes with VDT decomposition and properties of the elastic element) and not on the contributions of viscoelastic elements. The damage evolution laws are expressed in the same manner as Eq. 13 for each microplane, but in which $F_{V,D,T}$ don't represent the associated forces to the damage variables. This calculated damage affects all the modules of all the branches in the same manner.

Due to its simplicity and various capabilities, the internal approach is used in the present work. The viscoelasticity will be integrated using an implicit forward scheme. A scheme of the used approach is shown in Figure 2.

The Maxwell chain model used for the viscoelasticity yields the following equations (stress additivity, element equilibrium and behaviour):

$$\underline{\underline{\sigma}}^{tot} = \sum_m \underline{\underline{\sigma}}_m \qquad \text{(Eq. 15)}$$

For each viscoelastic element m, the strain is decomposed into elastic strain $\underline{\underline{\varepsilon}}^e_m$ and viscous strain $\underline{\underline{\varepsilon}}^v_m$, as follows:

$$\underline{\underline{\varepsilon}} = \underline{\underline{\varepsilon}}^e_m + \underline{\underline{\varepsilon}}^v_m \qquad \text{(Eq. 16)}$$

The stress continuity imposes:

$$\underline{\underline{\sigma}}_m = \underline{\underline{\sigma}}^e_m = \underline{\underline{\sigma}}^v_m \qquad \text{(Eq. 17)}$$

The behaviour inside the elements is described by:

$\underline{\underline{\sigma}}^{e}_{m} = \underline{\underline{\underline{\underline{C}}}}^{d}_{m} : \underline{\underline{\varepsilon}}^{e}_{m}$ and $\underline{\underline{\sigma}}^{v}_{m} = \eta_{m} : \underline{\underline{\dot{\varepsilon}}}^{v}_{m}$ for the elasticity and viscosity respectively.

Using the previous equations, the following development was made for every element *m*:

$$\underline{\underline{\varepsilon}}_{n+1} = \underline{\underline{\varepsilon}}_{n} + \Delta\underline{\underline{\varepsilon}}$$

From (Eq. 16), we can write:

$$\underline{\underline{\varepsilon}}_{n+1} = \underline{\underline{\varepsilon}}^{e}_{n+1} + \underline{\underline{\varepsilon}}^{v}_{n+1} = \underline{\underline{\varepsilon}}^{e}_{n} + \Delta\underline{\underline{\varepsilon}}^{e} + \underline{\underline{\varepsilon}}^{v}_{n} + \Delta\underline{\underline{\varepsilon}}^{v}$$

$$\Rightarrow \Delta\underline{\underline{\varepsilon}}^{v} = \underline{\underline{\varepsilon}}_{n} + \Delta\underline{\underline{\varepsilon}} - \left(\underline{\underline{\varepsilon}}^{e}_{n} + \Delta\underline{\underline{\varepsilon}}^{e}\right) - \underline{\underline{\varepsilon}}^{v}_{n}$$

Also, we obtain from (Eq. 17):

$$\underline{\underline{\sigma}}_{n+1} = \eta\frac{\Delta\underline{\underline{\varepsilon}}^{v}}{\Delta t} = \frac{\eta}{\Delta t}\left(\underline{\underline{\varepsilon}}_{n} + \Delta\underline{\underline{\varepsilon}} - \underline{\underline{\varepsilon}}^{e}_{n+1} - \underline{\underline{\varepsilon}}^{v}_{n}\right) = \underline{\underline{\underline{\underline{C}}}}^{d}_{n+1} : \underline{\underline{\varepsilon}}^{e}_{n+1}$$

$$\Rightarrow \underline{\underline{\varepsilon}}^{e}_{n+1} = \left(\underline{\underline{\underline{\underline{C}}}}^{d}_{n+1} + \frac{\eta}{\Delta t}\underline{\underline{\underline{\underline{I}}}}\right)^{-1} \times \frac{\eta}{\Delta t}\left(\underline{\underline{\varepsilon}}^{e}_{n} + \Delta\underline{\underline{\varepsilon}}\right), \qquad \text{(Eq. 18)}$$

where *n* and *n+1* denote respectively the beginning and the end of an increment. To integrate the viscoelasticity inside the microplanes, as stated by the internal approach, the expression of the elastic strain in each viscoelastic element (Eq. 18) is projected on the microplanes *i* following V-D-T decomposition:

$$\varepsilon^{e^{Volumetric}}_{m_{n+1}} = \left(\frac{\eta^{Volumetric}_{m}}{\Delta t \times E^{Volumetric}_{m} \times \left(1 - \alpha^{Volumetric} \times d^{Volumetric}\right) + \eta^{Volumetric}_{m}}\right) \times \left(\varepsilon^{e^{Volumetric}}_{m_{n}} + \Delta\varepsilon^{Volumetric}\right), \text{ (Eq. 19)}$$

$$\varepsilon^{e^{Deviatoric}}_{i_{m_{n+1}}} = \left(\frac{\eta^{Deviatoric}_{m}}{\Delta t \times E^{Deviatroic}_{m} \times \left(1 - \alpha^{Deviatoric}_{i} \times d^{Deviatoric}_{i}\right) + \eta^{Deviatoric}_{m}}\right) \times \left(\varepsilon^{e^{Deviatoric}}_{i_{m_{n+1}}} + \Delta\varepsilon^{Deviatoric}_{i}\right), \quad \text{(Eq. 20)}$$

$$\underline{\varepsilon}^{e^{Tangential}}_{i_{m_{n+1}}} = \left(\frac{\eta^{Tangential}_{m}}{\Delta t \times E^{Deviatroic}_{m} \times \left(1 - \alpha^{Tangential}_{i} \times d^{Tangential}_{i}\right) + \eta^{Tangential}_{m}}\right) \times \left(\underline{\varepsilon}^{e^{Tangential}}_{i_{m_{n+1}}} + \underline{\Delta\varepsilon}^{Tangential}_{i}\right), \text{ (Eq. 21)}$$

with η denoting the viscosity and $\eta^{Deviatoric}_{m} = \eta^{Tangential}_{m} \neq \eta^{Volumetric}_{m}$.

The Microplane model is very computationally demanding, mainly because it deals with all microstress components. In the literature, some authors presented a comprehensive study on the numerical aspects of a class of microplane constitutive models for concrete with emphasis on the most popular one, i.e., the model M4 (Bazant, et al., 2000) (Caner & Bazant, 2000).

It was observed that the Microplane model leads to numerical results that are sensitive to the strain increment magnitude (Huang, et al., 2017) (Nemecek, et al., 2002), which can cause an excessive lateral expansion on the macroscale level instead of contraction in the evaluated

uniaxial tension tests (Nemecek, et al., 2002). The algorithm gives different responses for small and large strain increments especially in the softening branches of macroscopic stress–strain curves.

Many studies (Qiu & Crouch, 1997) (Nemecek, et al., 2002) (Badel & Leblond, 2004) (Ehret, et al., 2010) (Levasseur, et al., 2013) (Verron, 2015) examined also the effect of the integration formula, number and distribution of the integration points on the unit sphere, on the performance of different Microplane models. It was found that the integration formula has an important impact on the predictions of the models and this effect depends on the number and the distribution of the integration points. The integration scheme usually adopted is a Gaussian integration with 21 or 28 points, developed by Bazant and Oh (Bazant & Oh, 1986). Di Luzio (Di Luzio, 2007) and Huang et al. (Huang, et al., 2017) reported that the numerical predictions of the Microplane model M4 depend on the loading directions when rotating the axes defining the position of the microplanes on the unit sphere. With a uniaxial compression test, in which displacements were applied in three orthogonal directions respectively, Di Luzio (Di Luzio, 2007) obtained different stress-strain curves. Huang et al. re-exanimed the influence of the loading direction on the response of the model using a more general approach, in which the axes (*x, y, z*) defining the position of the microplanes on the unit sphere are subjected to rotation while the loading direction remains constant. The following 21, 28, 37 and 61-points integration formulas and 4 different orientations were considered. For each considered integration formula, different loading directions lead to different stress-strain curves (Huang, et al., 2017). The dependence of the model responses on the loading direction mainly results from the directional behaviour of the used integration formula induced by the uneven distribution of the microplanes over the unit sphere (Huang, et al., 2017). This numerical sensitivity of the Microplane models can affect their ability to reflect the isotropy or anisotropy of the considered constitutive equation and its ability to integrate non-smooth functions (Badel & Leblond, 2004) (Verron, 2015) (Ehret, et al., 2010). With the increase of the number of the integration point, the difference with the predicted stress–strain curves generally decreases. Among the most classical integration formulas, the 61-point one is recommended to be used in numerical simulations. Some authors suggested that the best strategy to numerically integrate functions of one variable exhibiting quick variations is not to use high-order Gaussian integration, but simply to subdivide the integration interval into many sub-intervals and use low-order Gaussian integration over each of them. Transposed to integration over some surface, this strategy consists in meshing this surface (Badel &

Leblond, 2004) (Levasseur, et al., 2013). Unfortunately, the price to pay for is an increase of the number of integration points (120 points seem necessary to converge well in the proposed problem), imposing an increase of the number of state variables that need to be stored and updated at each loading step.

In this study, in one hand, the influence of the strain increment on the predictions from our model is examined in uniaxial compression using finite element simulations on a cube. Four step increment values are used: 10, 1, 0.1 and 0.01. In the other hand, to evaluate the influence of the loading direction, uniaxial compression simulations were run with 26 different orientations over the ¼ of the hemisphere. The 26 different orientations of solicitation are extracted from a sphere surface meshed with 162 directions (same weight), keeping only those contained in ¼ of the hemisphere. The simulated cube is rotated with the loading direction while the axes (*x, y, z*) remain constant. The cube is rotated by an angle α along the axis *y*, followed by a second rotation by an angle β along the new axis *z*. For the loading direction sensitivity, three different integration formulas were considered from the literature (Bazant & Oh, 1986) (Badel & Leblond, 2004). The details and the results are presented and analysed in section 5.

3.3 Parameters identification

The viscoelastic parameters could be identified with the previously fixed damage parameters. These damage parameters were identified by fitting the curve "extended experimental relaxed points" with elastic damaged Microplane model predictions (Figure 3 and 4). Extended experimental relaxed points were obtained by eliminating temporal contributions, so the resulted points are supposed to represent an elastic damaged behaviour. The initial viscoelastic modules were obtained from (Le, et al. 2010) and then were iteratively adjusted to fit the relaxation steps, in tension and compression (Figure 7 and 8). To simplify the parameters identification process, values already used in (Picart, et al., 2014) (Le, et al., 2010) and (Caliez, et al., 2014) were considered in the beginning. The initial experimental elastic modulus and viscous moduli of the material were identified from DMA tests, at 20°C (Le, et al., 2010). This initial elastic modulus was adjusted, based on the comparison between simulation results obtained using the damaged elastic Microplane model and the reconstructed experimental stress-strain (σ-ε) curves obtained by extending the relaxation steps. In fact, to insure a complete stress relaxation, the time step was extended from 1800 s, for cyclic compression, and from 3000 s, for cyclic tension, to 10^4 s. Figure 3 and Figure 4

show the original relaxed points and the extended relaxed points for compression and tension tests performed at a strain rate of 3.3×10^{-5}/s. The elastic modulus was adjusted to better fit both tension and compression experimental data. The obtained value is E = 2400 MPa. Experimentally, initial Poisson's ratio ranges between 0.25 and 0.4 for tension and compression tests (Le, et al., 2010) (Caliez, et al., 2014). A value of 0.4 was considered for this model. Damage parameters were also adjusted to capture experimental extended relaxed points with the damaged elastic Microplane model. The obtained values are given in Table 1.
After calibrating initial elastic modulus and damage parameters with the damaged elastic Microplane model, viscous moduli initially obtained from DMA tests (Le, et al., 2010) are adjusted regarding the best fit between predictions for cyclic compression and tension obtained with the developed viscoelastic Microplane model and experimental results, in terms of longitudinal stress in relaxation steps. Relaxation times are kept identical as in (Le, et al., 2010) without adjustment. It is to be noted that the first four viscous moduli do not significantly affect the simulations results for the strain rates considered in this paper. The viscous moduli and the relaxation times used in our model are reported in Table 2. Relaxation times were defined to guarantee an almost complete relaxation of the stress from quasi-static to slow dynamic solicitations (Le, et al., 2010).

4 Validation of the viscoelastic Microplane model

The viscoelastic behaviour was taken into account in the Microplane approach and the resulting model was successfully implemented in the commercial finite element software "Abaqus", using Umats and following the internal approach described above. The standard 21 symmetric directions on a hemisphere, proposed by Bazant and Oh (Bazant & Oh, 1986), were used to define the directions of microplanes. A 3-dimensional, 8 nodes element with a reduced integration (element C3D8R) was considered. The model is simple and fast to be implemented, since variables are projected on the microplanes and, so, only scalar variables or vectors are managed. However, it requires many state variables to be saved (~900 SDV in this study), which makes the simulation times consuming. Cyclic σ-ε curves are reported in Figure 5 and Figure 6, globally showing a good agreement between experimental results and numerical simulations, in both longitudinal and transversal directions. However, the proposed model still lacks accuracy when simulating unloading paths and strain evolution in recovery steps, in compression loadings, even if the experimental tendencies are well predicted.

Figure 7 and Figure 8 show experimental and numerical longitudinal stress evolutions, in relaxation steps, respectively, in cyclic compression and cyclic tension. The numerical predictions are globally consistent with experimental data with a better fit being obtained in compression. This is probably due to the fact that the compression experimental results were favoured in the adjustment process of the damage parameters (Figure 3 and Figure 4).

To evaluate the model at different strain rates, monotonic compression tests with strain rates of 8.3×10^{-4} s^{-1}, 3.3×10^{-5} s^{-1} and 4.4×10^{-6} s^{-1} were simulated and the results are compared to experimental data, respectively to the strain rate, in Figure 9, Figure 10 and Figure 11. Despite some slight divergence, reaching a maximum of ~11% between numerical and experimental curves, the proposed viscoelastic Microplane model reproduces the strain rate effect.

5 Numerical aspects of the model

To test the sensitivity of the proposed Microplane model on the strain increment, four simulations of the monotonic compression test were run at a strain rate of 3.3×10^{-5} with four different step increments: 10, 1, 0.1, and 0.01 corresponding respectively to strain increments of 3.3×10^{-4}, 3.3×10^{-5}, 3.3×10^{-6} and 3.3×10^{-7}. The model was reduced to only one viscoelastic element and one elastic element so as to reduce CPU time. For this study, the standard 21 symmetric directions on a hemisphere, proposed by Bazant and Oh (Bazant & Oh, 1986), were used to define the directions of microplanes. The simulations were stopped at the peak of the stress since the behaviour of the material at the softening phase is out of the focus of the present work. The results presented in Figure 12 do not show any remarkable sensitivity to the strain increment, particularly in the linear regime.

An almost perfect convergence is obtained between the simulations at strain increments of 3.3×10^{-6} and 3.3×10^{-7} which is consistent with the finding of (Nemecek, et al., 2002). The strain increment of 3.3×10^{-6} seems to be the critical value that ensures the best convergence and the stability of the model. In our study however, bigger step increments are acceptable since the behaviour of the material in the softening phase is not important.

The literature already highlighted the sensitivity of the Microplane models to the loading orientation as mentioned above. In this study, we performed simulations with 26 different orientations over the ¼ of the hemisphere, where the simulated cube is rotated with the loading direction while the axes (*x, y, z*) remain constant using integration formulas with 21-, 61-points, as proposed by (Bazant & Oh, 1986), and 362 points obtained from a sphere

surface meshing, as proposed by (Badel & Leblond, 2004). With 21 points, a maximal divergence of 3.6% is obtained between the maximum and the minimum longitudinal stresses, in the last increment of the simulation (Figure 13). This divergence could be greater when simulating structures with many elements. Using the 61-point integration formula, the maximal divergence is reduced to 0.64% (Figure 14). In Figure 15, stress-strain curves were obtained with 362-points integration formula. All the Microplanes have the same weight ($w=1/362$). The maximal divergence is of 0.26%. The results mentioned above indicate the following findings:

- Different loading directions lead to more or less dispersion in the predicted stress-strain curves for the used integration schemes;
- When increasing the number of the integration point, the dispersion of the stress-strain curves is reduced;
- The 61-point integration formula seems to be adequate for our model and extending to the 362-point configuration is unnecessary based on the obtained results.

Conclusion

A new viscoelastic Microplane model has been proposed to simulate the behaviour of quasi-brittle PBX materials, using a Maxwell chain model and the Microplane approach. The integration of both the viscoelasticity and the damage induced anisotropy represents one of the new contributions of this work for such kinds of materials.

The modelling approach consists in integrating a viscoelastic model in each microplane where the components of elastic strains are projected on the microplane directions following a V-D-T decomposition.

It appeared that the numerical predictions reasonably fitted experimental data, when considering the envelope curve, the transversal strain and the relaxation steps. Moreover, the effect of the strain rate on the material mechanical response seems to be quite well supported by the model. However, the proposed model still lacks accuracy when simulating unloading path in compression and strain evolution in recovery steps. As a perspective of this study, irreversible strain will be considered in our future investigations (plasticity or friction between microcracks lips).

The model shows a small sensitivity to the strain increment though a good convergence is globally obtained. Different loading directions lead to more or less dispersion in the predicted stress-strain curves for the used integration formulas. The 21-point integration formula is

insufficient to minimize the influence of the loading direction on the results. The 61-point configuration seems to be a good compromise between the accuracy of the results, state variables and the CPU time.

Acknowledgements. Authors thank "Région Centre Val de Loire, France" and "INSA Centre Val de Loire, France" for funding this project.

References

Badel, P. B. & Leblond, J. B., 2004. A note on integration schemes for the microplane model of the mechanical behaviour of concrete. *Communications in numerical methods in engineering,* Volume 20, pp. 75-81.

Bargellini, R., 2006. *Contribution d'une approche discrète à la modélisation de l'endommagement de matériaux microfissurés.* Poitiers: Ecole nationale supérieure de mécanique et d'aérotechnique.

Bargellini, R., Halm, D. & Dragon, A., 2008. Modelling of quasi-brittle behaviour: a discrete approach coupling anisotropic damage growth and frictional sliding. *European Journal of Mechanics,* 27(4), pp. 564-581.

Batdorf, S. B. & Budiansky, B., 1949. *A mathematical theory of plasticity based on the concept on the concept of slip,* s.l.: National Advisory Committee for Aeronautics.

Bazant, Z. P., Caner, F. C., Adley, M. D. & Akers, S. A., 2000. Fracturing rate effect and creep in Microplane model for dynamics. *Journal of Engineering Mechanics,* 126(9), pp. 962-970.

Bazant, Z. P. et al., 2000. Microplane Model M4 for concrete. I: Formulation with work-conjugate deviatoric stress. *Journal of Engineering Mechanics,* 126(9), pp. 944-953.

Bazant, Z. P. & Gambarova, P. G., 1984. Crack shear in concrete: Crack band microplane model. *Journal of structural engineering,* Volume 110, pp. 2015-2035.

Bazant, Z. P. & Oh, B. H., 1986. Efficient numerical integration on the surface of a sphere. *ZAMM-Journal of Applied Mathematics and Mechanics/Zeitschrift für Angewandte Mathematik und Mechanik,* 66(1), pp. 37-49.

Belmas, R., Reynaud, J. & Sorel, J., 1982. Simulation numérique du comportement viscoélastique non-linéaire d'un matériau explosif. *Propellants, Explosives, Pyrotechnics,* 7(1), pp. 8-11.

Benelfellah, A. et al., 2014. Analytical and numerical comparison of discrete damage models with induced anisotropy. *Engineering Fracture Mechanics,* Volume 121, pp. 28-39.

Bennett, J. G., Haberman, K. S., Johnson, J. N. & Asay, B. W., 1998. A constitutive model for the non shock ignition and mechanical response of high explosives. *Journal of the Mechanics and Physics of Solids,* 46(12), pp. 2303-2322.

Caliez, M. et al., 2014. Viscoelastic plastic model and experimental validation for a granular energetic material. *International Journal of Energetic Materials and Chemical Propulsion,* 13(4), pp. 339-371.

Caner, F. C. & Bazant, Z. P., 2000. Microplane Model M4 for concrete. II: Algorithm and calibration. *Journal of Engineering Mechanics,* 126(9), pp. 954-961.

Carol, I., Jiràsek, M. & Bazant, Z. P., 2001. A thermodynamically consistent approach to microplane theory. Part I. Free energy and consistent microplane stresses. *International Journal of Solids and Structures,* 38(17), pp. 2921-2931.

Carol, I. & Willam, K., 1996. Spurious energy dissipation/generation in stiffness recovery models for elastic degradation and damage. *International Journal of Solids and Structures,* 33(20-22), pp. 2939-2957.

Challamel, N., Halm, D. & Dragon, A., 2006. On the non-conservativeness of a class of anisotropic damage models with unilateral effects. *Comptes Rendus Mecanique,* 334(7), pp. 414-418.

Chen, P., Huang, F. & Ding, Y., 2007. Microstructure, deformation and failure of polymer bonded explosives. *Journal of materials science,* 42(13), pp. 5272-5280.

Cormery, F. & Welemane, H., 2002. A critical review of some damage models with unilateral effect. *Mechanics Research Communications,* 29(5), p. 391–395.

Di Luzio, G., 2007. A symmetric over-nonlocal microplane model M4 for fracture in concrete. *International Journal of Solids and Structures,* 44(13), pp. 4418-4441.

Di Luzio, G., 2009. Numerical model for time-dependent fracturing of concrete. *Journal of Engineering Mechanics,* 135(7), pp. 632-640.

Di Luzio, G. & Cedolin, L., 2007. *Numerical model for time-dependent fracturing of concrete structures and its application.* Catania, Italy, s.n., pp. 175-180.

Dienes, J. K., 1982. *Permeability, percolation and statistical crack mechanics.* Berkeley, California, American Rock Mechanics Association.

Dienes, J. K., 1996. A unified theory of flow, hot spots, and fragmentation with an application to explosive sensitivity. Dans: *High-Pressure Shock Compression of Solids II.* New York: Springer, p. 366–398.

Dienes, J. K., Zuo, Q. H. & Kershner, J. D., 2006. Impact initiation of explosives and propellants via statistical crack mechanics. *Journal of the Mechanics and Physics of Solids,* 54(6), pp. 1237-1275.

Ehret, A. E., Itskov, M. & Schmid, H., 2010. Numerical integration on the sphere and its effect on the material symmetry of constitutive equations - A comparative study. *International Journal for Numerical Methods in Engineering,* 81(2), pp. 189-206.

Ellis, K., Leppard, C. & Radesk, H., 2005. Mechanical properties and damage evolution of a UK PBX. *Journal of materials science,* 40(23), pp. 6241-6248.

Gratton, M. et al., 2009. Mechanical characterization of a viscoplastic material sensitive to hydrostatic pressure. *European Journal of Mechanics - A/Solids,* 28(5), pp. 935-947.

Hackett, R. M. & Bennett, J. G., 2000. An implicit finite element material model for energetic particulate composite materials. *International Journal for Numerical Methods in Engineering,* 49(9), pp. 1191-1209.

Ha, K. & Schapery, R. A., 1998. A three-dimensional viscoelastic constitutive model for particulate composites with growing damage and its experimental validation. *International Journal of Solids and Structures,* 35(26-27), pp. 3497-3517.

Hasegawa, T. & Bazant, Z. P., 1993. Nonlocal microplane concrete model with rate effect and load cycles. I: General formulation. *Journal of Materials in Civil Engineering,* 5(3), pp. 372-393.

Huang, L. C. et al., 2017. Numerical aspects of microplane constitutive models for concrete. *Applied Mathematical Modelling,* Volume 41, pp. 530-548.

Kuhl, E., Steinmann, P. & Carol, I., 2001. A thermodynamically consistent approach to microplane theory. Part II. Dissipation and inelastic constitutive modeling. *International journal of solids and structures,* Volume 38, pp. 2933-2952.

Levasseur, S., Collin, F., Charlier , R. & Kondo, D., 2013. On micromechanical damage modeling in geomechanics: Influence of numerical integration scheme. *Journal of Computational and Applied Mathematics,* Volume 246, p. 215–224.

Le, V. D. et al., 2010. Experimental mechanical characterization of plastic-bonded explosives. *Journal of Materials Science,* 45(21), pp. 5802-5813.

Liu, Z. W. et al., 2009. Fracture behavior of PBX simulant subject to combined thermal and mechanical loads. *Polymer testing,* 28(6), pp. 627-635.

Maire, J. F. & Chaboche, J. L., 1997. A new formulation of continuum damage mechancis (CDM) for composite materials. *Aerospace Science and Technology,* 1(4), pp. 247-257.

Murakami, S. & Kamiya, K., 1997. Constitutive and damage evolution equations of elastic-brittle materials based on irreversible thermodynamics. *International Journal of Mechanical sciences,* 39(4), pp. 473-486.

Nemecek, J., Patzak, B., Rypl, D. & Bittnar, Z., 2002. Microplane models: computational aspects and proposed parallel algorithm. *Computers and Structures,* 80(27-30), pp. 2099-2108.

Ozbolt, J. & Bazant, Z. P., 1992. Microplane model for cyclic triaxial behavior of concrete. *Journal of Engineering Mechanics,* 118(7), pp. 1365-1386.

Ozbolt, J. & Reinhardt, H.-W., 2001. Sustained loading strength of concrete modelled by creep-cracking interaction. *Otto - Graf - Journal,* 12(9).

Pecqueur, G., 1995. *Étude expérimentale et modélisation du comportement d'une craie et d'un grès en torsion.* Lille: Université de Lille 1.

Picart, D. et al., 2014. Characterization and modeling of the anisotropic damage of a high-explosive composition. *Engineering Fracture Mechanics,* Volume 131, p. 525–537.

Qiu, Y. & Crouch, R. S., 1997. *Spurious compaction in the microplane model and a new adaptative framework.* Barelona, s.n., pp. 493-499.

Saadeh, S. A. R., 2005. *Characterization of asphalt concrete using anisotropic damage viscoelastic-viscoplastic model.* College Station, Texas: Texas A&M University.

Taylor, G. I., 1938. Plastic strains in metals. *Journal of the Institute of Metals,* Volume 62, pp. 307-324.

Trumel, H., Lambert, P. & Belmas, R., 2010. *Mesoscopic investigations of the deformation and initiation mechanisms of a hmx-based pressed composition.* Coeur d'Alene (ID), USA, s.n.

Verron, E., 2015. Questioning numerical integration methods for microsphere (and microplane) constitutive equations. *Mechanics of Materials,* Volume 89, pp. 216-228.

Williamson, D. M. et al., 2008. Temperature-time response of a polymer bonded explosive in compression (EDC37). *Journal of Physics D: Applied physics,* 41(8).

Xiao, Y., Sun, Y., Yang, Z. & Guo, L., 2017. Study of the dynamic mechanical behaviour of PBX by Eshelby theory. *Acta Mechanica,* 228(6), pp. 1993-2003.

Xiao, Y. et al., 2017. Characterization, modeling and simulation of the impact damage for polymer bonded explosives. *International Journal of Impact Engineering,* Volume 103, pp. 149-158.

Zhu, Q. Z., Shao, J. F. & Kondo, D., 2008. A micromechanics-based non-local anisotropic model for unilateral damage in brittle materials. *Comptes Rendus Mécanique,* 336(3), pp. 320-328.

Zi, G. & Bazant, Z. P., 2002. Continuous relaxation spectrum for concrete creep and its incorporation into Microplane model M4. *Journal of Engineering Mechanics,* 128(12), pp. 1331-1336.

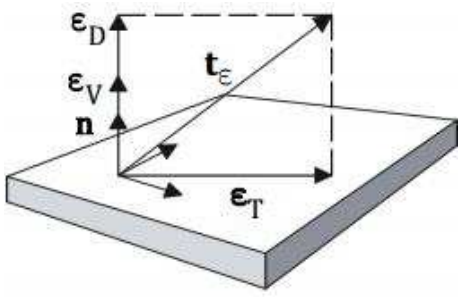

Figure 1. VDT decomposition in Microplane directions (Kuhl, et al., 2001)

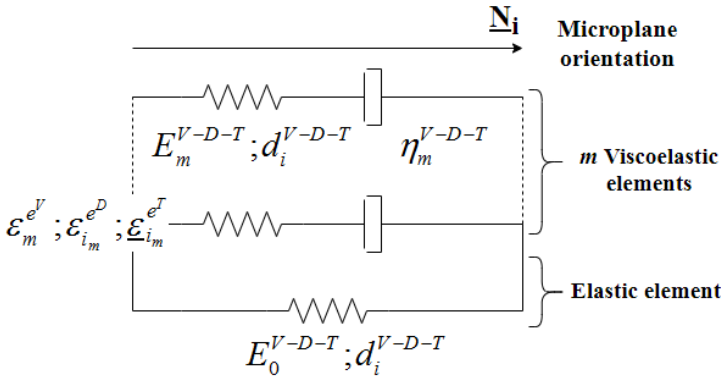

Figure 2. Internal approach scheme

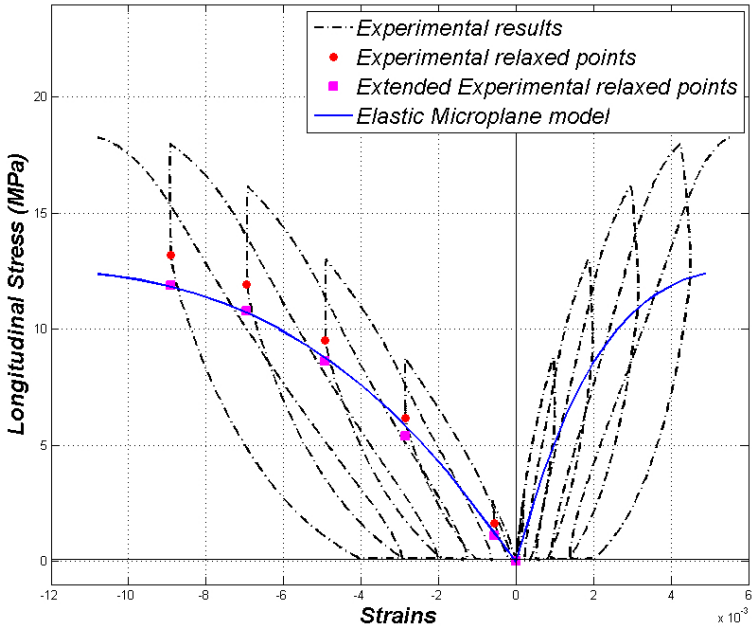

Figure 3. Calibrating damage parameters based on extended experimental relaxed points of cyclic compression

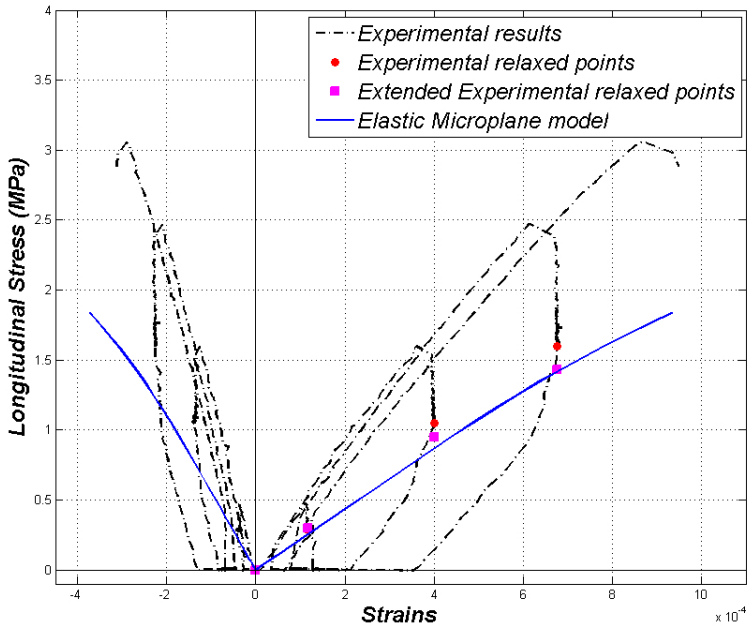

Figure 4. Calibrating damage parameters based on extended experimental relaxed points of cyclic tension

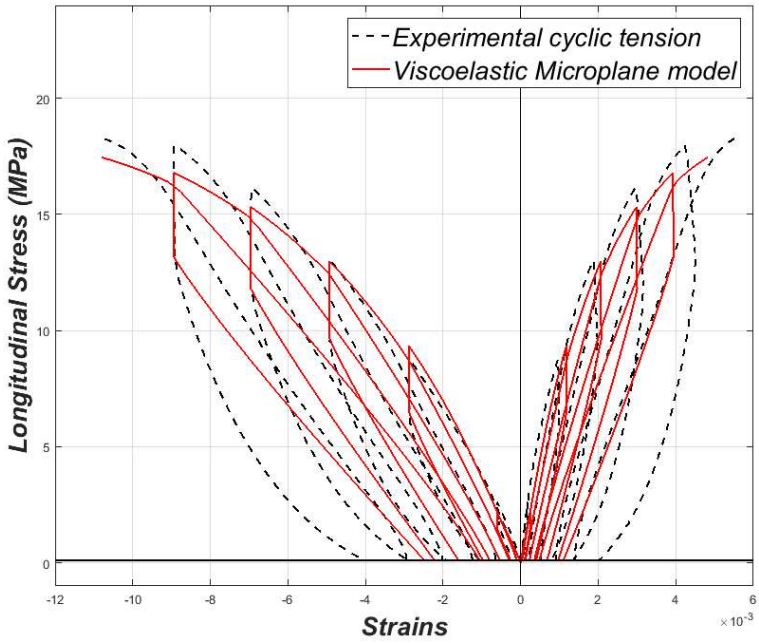

Figure 5. Experimental and numerical σ-ε curves of cyclic compression results.

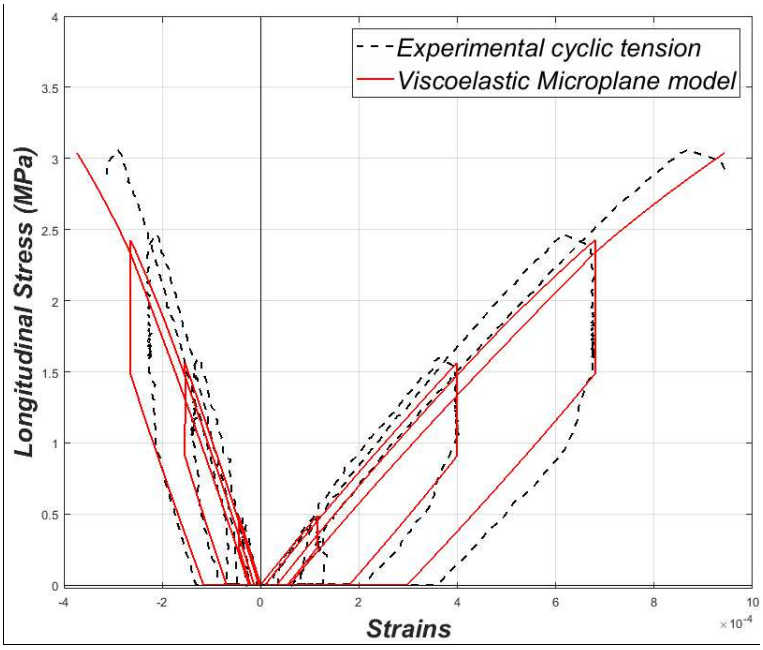

Figure 6. Experimental and numerical σ-ε curves of cyclic tension results

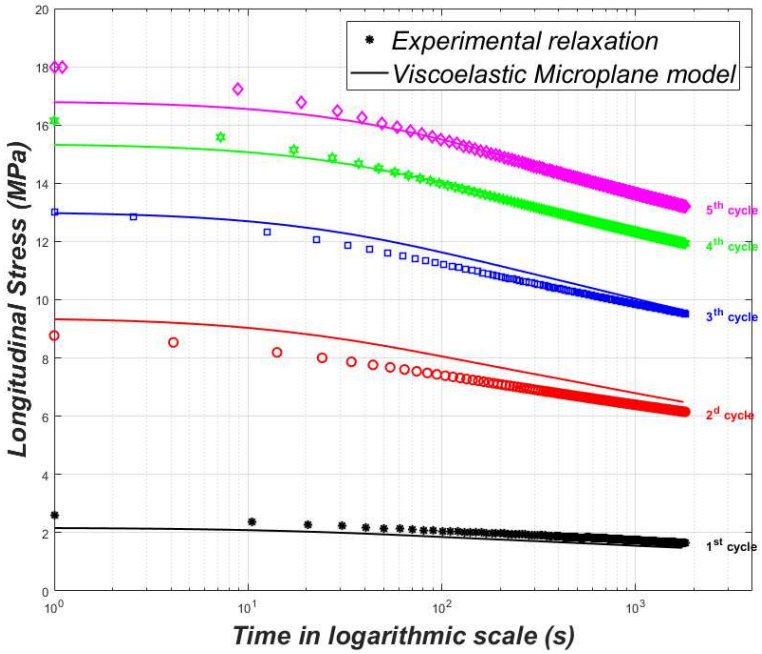

Figure 7. Experimental and numerical evolutions of longitudinal stress in relaxation steps of cyclic compression

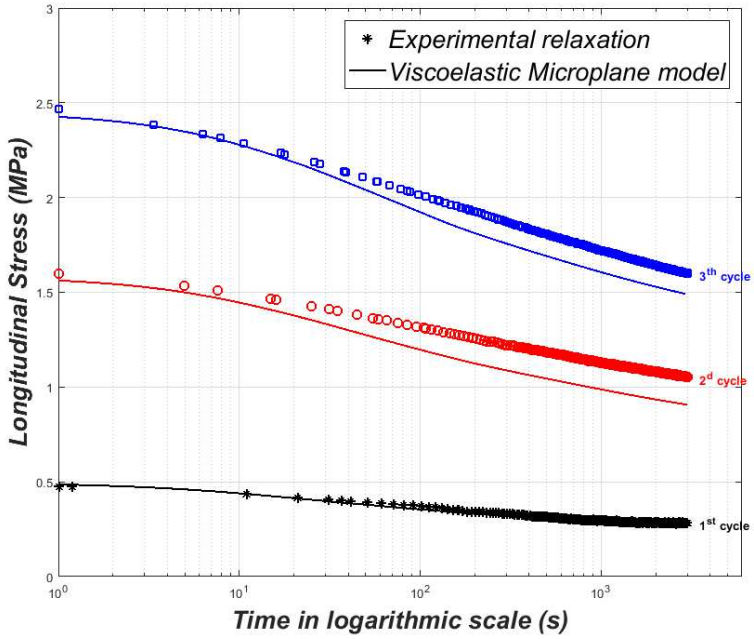

Figure 8. Experimental and numerical evolution of longitudinal stress in relaxation steps of cyclic tension

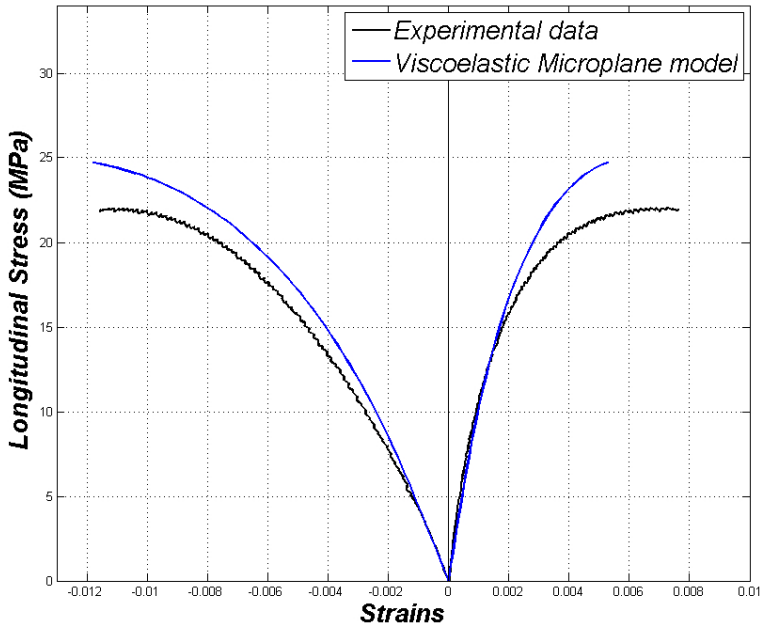

Figure 9. Experimental and numerical σ-ε curves of monotonic compression test, strain rate = 8.3×10^{-4}/s

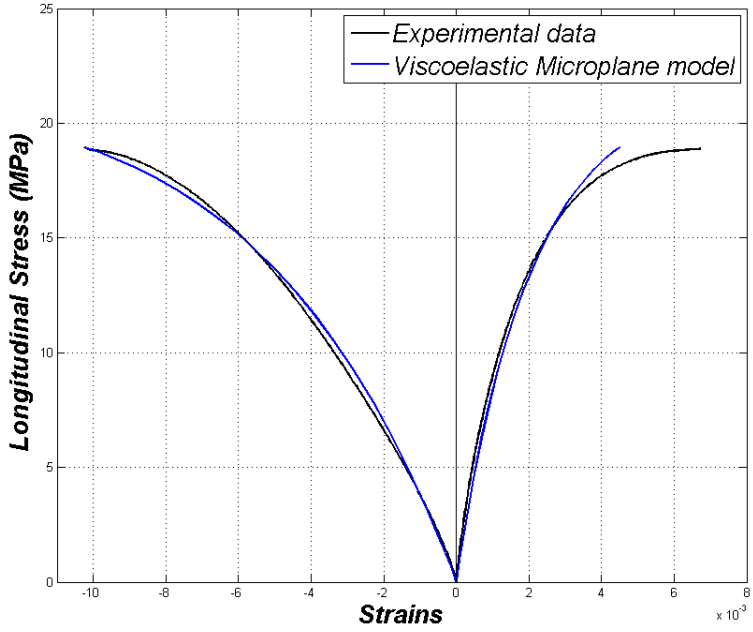

Figure 10. Experimental and numerical σ-ε curves of monotonic compression test, strain rate = 3.3×10^{-5}/s

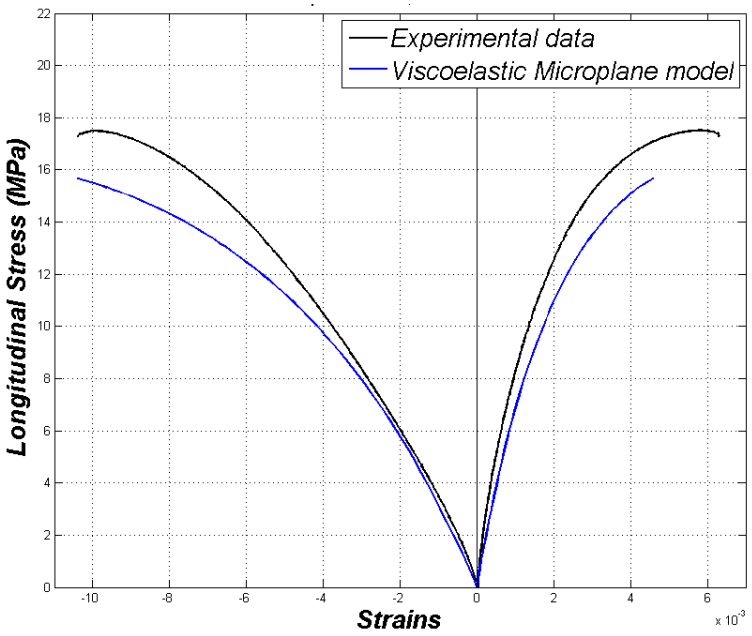

Figure 11. Experimental and numerical σ-ε curves of monotonic compression test, strain rate = 4.4×10^{-6}/s

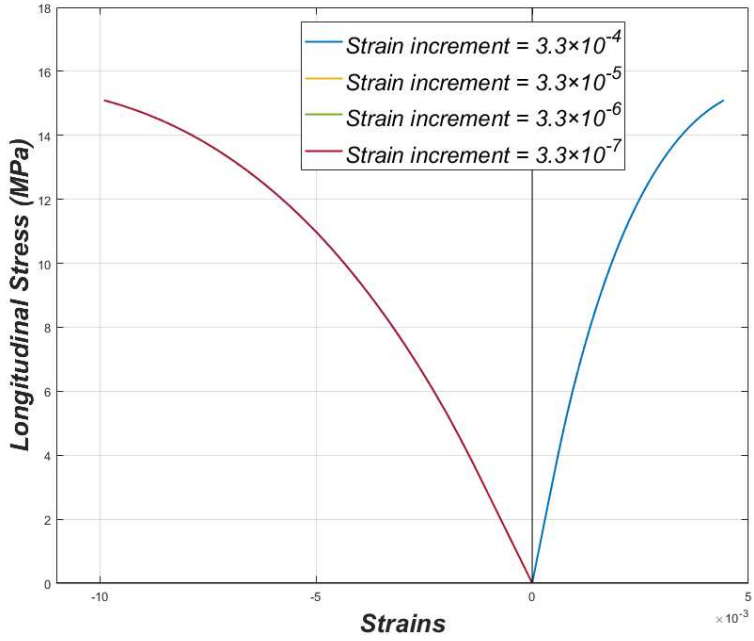

Figure 12. Dependence on the strain increment magnitude

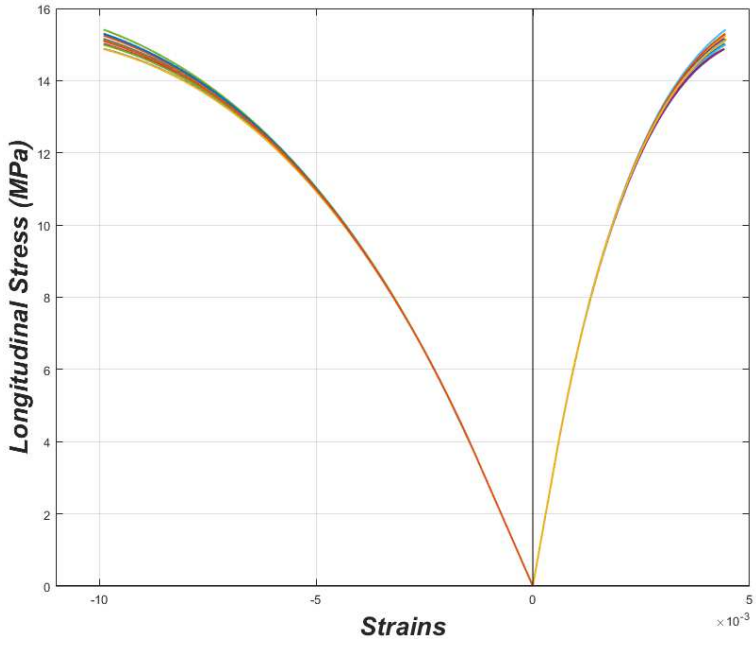

Figure 13. Impact of loading direction on the simulation results in compression with 21 microplanes

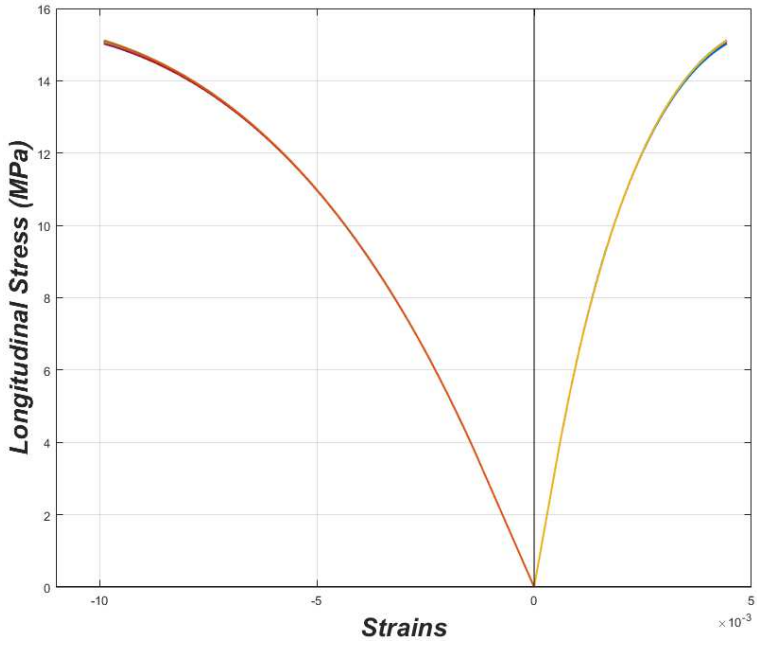

Figure 14. Impact of loading direction on the simulation results in compression with 61 microplanes

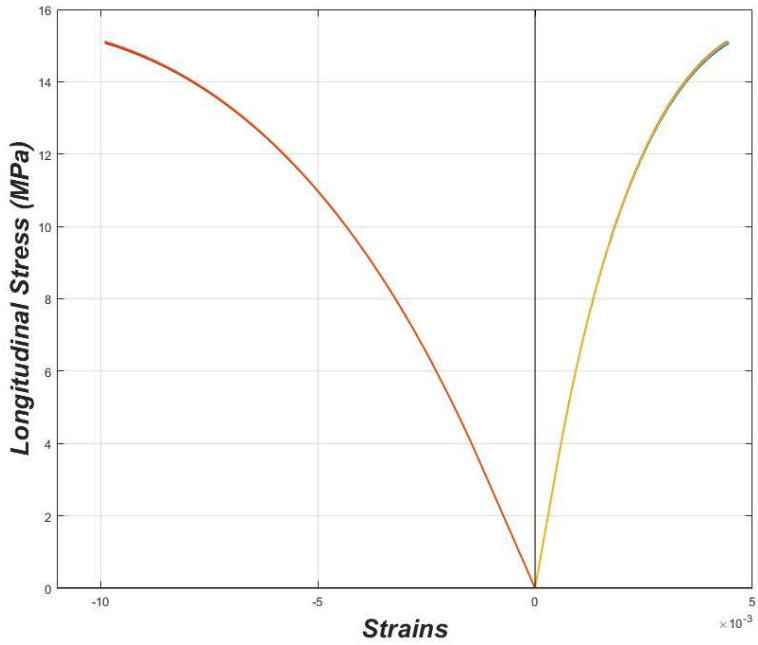

Figure 15. Impact of loading direction on the simulation results in compression with 362 microplanes

Table 1. Damage parameters used in the model

$a_1^{V,D}$	a_1^T	a_2	a_3	a_4	ε_V^{0-H10}
6	7.8	0.5	0.3	1.5	-8.309×10^{-4}

Table 2. Viscous parameters used in the model

Element m	1	2	3	4	5	6	7	8	9	10
τ_m *(sec)*	5×10^{-4}	29×10^{-4}	168×10^{-4}	0.098	0.567	3.28	19.05	110.5	640.7	3715
E_m *(MPa)*	546	336	240	348	60	40	692	752	392	588